

Decennial time trends and diurnal patterns of particle number concentrations in a Central European city between 2008 and 2018

Santtu Mikkonen^{1,2}, Zoltán Németh³, Veronika Varga³, Tamás Weidinger⁴, Ville Leinonen¹,
Taina Yli-Juuti¹, and Imre Salma³

¹ Department of Applied Physics, University of Eastern Finland, P.O. Box 1627, 70211 Kuopio, Finland

² Department of Environmental and Biological Sciences, University of Eastern Finland, P.O. Box 1627,
70211 Kuopio, Finland

³ Institute of Chemistry, Eötvös University, H-1518 Budapest, P.O. Box 32, Hungary

⁴ Department of Meteorology, Eötvös University, H-1518 Budapest, P.O. Box 32, Hungary

Correspondence to: Imre Salma (salma@chem.elte.hu) and Santtu Mikkonen (santtu.mikkonen@uef.fi)

Abstract. Multiple atmospheric properties were measured semi-continuously in the Budapest platform for Aerosol Research and Training Laboratory which represents the urban background for a time interval of 2008-2018. Dataset of 6 full measurement years during a decennial time interval were subjected to statistical time trend analyses by an advanced dynamic linear model and a generalized linear mixed model. The main interest in the analysed data set was on particle number concentrations in the diameter ranges from 6 to 1000 nm (N_{6-1000}), from 6 to 100 nm (N_{6-100} , ultrafine particles), from 25 to 100 nm (N_{25-100}) and from 100 to 1000 nm ($N_{100-1000}$). These data were supported by concentrations of SO₂, CO, NO, NO_x, O₃, PM₁₀ mass, air temperature, relative humidity, wind speed, atmospheric pressure, global solar radiation, condensation sink, gas-phase H₂SO₄ proxy, classes of new aerosol particle formation (NPF) and growth events and meteorological macro-circulation patterns. The trend of the particle number concentrations derived as a change in the statistical properties of background state of the data set decreased in all size fractions over the years. Most particle number concentrations showed decreasing decennial statistical trends. The estimated annual mean decline of N_{6-1000} was (4–5)% during the 10-year measurement interval, which corresponds to a mean absolute change of -590 cm^{-3} in a year. This was interpreted as a consequence of the decreased anthropogenic emissions at least partly from road traffic alongside to household heating and industry. Similar trends were not observed for the air pollutant gases. Diurnal statistical patterns of particle number concentrations showed tendentious variations, which were associated with typical diurnal activity–time pattern of inhabitants in cities, particularly of vehicular road traffic. The trend patterns for NPF event days contained a huge peak from late morning to late afternoon, which is unambiguously caused by NPF and growth processes. These peaks were rather similar to each other in the position, shape and area on workdays and holidays, which implies that the dynamic and timing properties of NPF events are not substantially influenced by anthropogenic activities in central Budapest. Diurnal pattern for N_{25-100} exhibited the largest relative changes, which were related to particle emissions from high-temperature sources. The diurnal pattern for $N_{100-1000}$ – which represents chemically and physically aged particles of larger spatial scale – were different from the diurnal patterns for the other size fractions.

37 **1 Introduction**

38 Atmospheric aerosol can be characterised by various properties. There are several important phenomena
39 and processes in which individual particles play a role. In these cases, particle number concentrations
40 or particle number size distributions are the relevant metrics. Number concentrations of (insoluble)
41 particles produce adverse effects on human health (Oberdörster et al., 2005; Rich et al., 2012; Cassee et
42 al., 2013; Braakhuis et al., 2014; Ostro et al., 2015; Schmid and Stoeger, 2016; Ohlwein et al., 2019).
43 Individual particles and their properties are also important in cloud formation processes and, therefore,
44 in indirect aerosol climate forcing (Makkonen et al., 2009; Merikanto et al., 2009; Sihto et al., 2011;
45 Kerminen et al., 2012; Carslaw et al., 2013; Gordon et al., 2016). Particle numbers and associated size
46 distributions are relevant properties in several optical interactions in the atmosphere (e.g. Moosmüller
47 et al., 2009) and in various surface-controlled chemical reactions (e.g. Pöschl et al., 2007).

48 In the global troposphere, it is the new aerosol particle formation (NPF) and consecutive growth process
49 that is the dominant source of particle numbers (Spracklen et al., 2006; Yu et al., 2010; Kulmala et al.,
50 2013; Dunne et al., 2016). This source type occurs in various atmospheric environments around the
51 world and produces secondary particles (Kerminen et al., 2018 and references therein). The major
52 anthropogenic source of (primary) particles is combustion. It includes traffic exhaust mainly from diesel
53 engines, fuel or waste burning in industrial and domestic installations, residential heating and cooking
54 (Paasonen et al., 2016; Masiol et al., 2018). Nanotechnology and its products can have importance in
55 some limited or occupational environments. In large cities and in longer time intervals, primary particles
56 often prevail over secondary particles (Brines et al., 2015; Salma et al., 2017; Saha et al., 2018).

57 Ultrafine (UF) particles (with a diameter $d < 100$ nm) account for most of the particle number
58 concentrations but have usually negligible contribution to particulate matter (PM) mass. This implies
59 that particle numbers are not covered by legislative regulations on the ambient air quality, which are
60 ordinary based on the PM mass. Particle number concentrations have not been promulgated among the
61 air quality standards yet. There are, however, mitigation policies and control regulations, which intend
62 to reduce their ambient levels as part of an overall air-quality improvement strategy since 1990s. The
63 legislations, for instance in the EU including Hungary, focus on the particle emissions from diesel
64 engines (Giechaskiel et al., 2018). There were some important changes in the car emissions during the
65 time interval under the investigation in this study. These included the introduction of Euro 5 and 6
66 regulations for light-duty vehicles in January 2011 and Euro VI regulations for heavy-duty vehicles in
67 September 2015 (the number of emitted particles with diameters > 23 nm should be $< 6 \times 10^{11}$ km⁻¹ for
68 type approval). A prerequisite for the efficient operation of exhaust after treatment devices is having
69 fuel with low sulfur content. The reduction of sulfur in diesel fuel for on-road transport was decreased
70 after several previous phases to < 10 ppm in January 2009 (Directive 2009/30/EC). Sulfur content in
71 fuels for mobile non-road diesel vehicles – including mobile machinery, agricultural and forestry

72 tractors, inland waterway vessels and recreational crafts – was limited at a level of 1000 ppm from 2008
73 and at 10 ppm from 2011. The unsuitable/dangerous fuel types for domestic heating are also listed, their
74 emission factors are determined, and the accumulated information is disseminated among potential
75 users. As far as secondary particles are concerned, it is not straightforward to reduce their concentration
76 levels because the effects of gaseous and aerosol species on the NPF are complex and uncertain due to
77 nonlinear relationship and feedbacks in their related processes.

78 It is relevant to investigate the potential changes, namely overall and diurnal tendencies of particle
79 number concentrations from different sources on longer run because of their role in both health-risk and
80 climate-change issues. The major source types of particle numbers can be separated by measuring their
81 size distributions. Atmospheric NPF events produce particles of the nucleation mode, which occurs
82 intermittently, and which gradually merges into the larger Aitken mode. High temperature emission
83 sources ordinarily produce Aitken-mode particles, while transformation processes (physical and
84 chemical aging) of existing particles in the atmosphere give rise to the accumulation mode. An important
85 property of the nucleation- and Aitken-mode particles is that their residence time is limited to several
86 hours (Raes et al., 2000; Salma et al., 2011). This is different from accumulation-mode particles, which
87 reside in the air up to 7 days. This means that the particles of the former two modes are present in the
88 air until their sources are active, and that their concentrations can change substantially and rapidly over
89 a day (e.g. Mikkonen et al., 2011a, Salma et al., 2014, 2017; Paasonen et al., 2016). This is advantageous
90 when source types are to be identified or quantified. At the same time, the relatively short residence time
91 is not beneficial when time trends are to be studied and derived. The limited residence time can cause
92 additional, substantial and sudden variability in time with or without time patterns, which can complicate
93 the evaluation.

94 Particle number concentrations or particle number size distributions in the relevant diameter range (i.e.
95 from few nanometers to ca. 1 μm) are measured for various purposes. They include fundamental studies
96 on atmospheric nucleation and particle growth phenomena, which usually require semi-continuous long-
97 term measurements. The related experimental data sets have been accumulating gradually (Wehner and
98 Wiedensohler, 2003; Asmi et al., 2013; Kerminen et al., 2018; Nieminen et al., 2018). They can also be
99 exploited for time trend analysis by using appropriate statistical models. At present, however, knowledge
100 on time trends particularly in various size fractions and over several years is largely lacking with few
101 recent exceptions (Masiol et al., 2018; Saha et al., 2018; Sun et al., 2020).

102 Research activities dedicated to NPF and growth events in Budapest have been going on since November
103 2008. Measurements for 6 full years were realised in the city centre at a single fixed location. Semi-
104 continuous and critically evaluated data sets consisting of particle number size distributions,
105 concentrations of criteria air pollutants and meteorological data were available for the study. They were
106 combined in a coherent set, which was utilised in two statistical models developed specifically to

107 determine the time trends for particle number concentrations in several important size fractions from
108 2008 to 2018. The main objectives of this study are to present and discuss the statistical models, to
109 interpret their results on time trends and diurnal variability, to quantify the change rates, and to relate
110 the temporal tendencies to different atmospheric sources, processes and environmental circumstances.

111 **2 Methods**

112 **2.1 Measurements**

113 Most experimental data dealt with in the present study were obtained at a single urban site, namely at
114 the Budapest platform for Aerosol Research and Training (BpART) research laboratory (N 47° 28' 29.9",
115 E 19° 3' 44.6", 115 m above mean sea level). This location represents a well-mixed, average atmospheric
116 environment for the city centre of Budapest due to its geographical and meteorological conditions
117 (Salma et al., 2016a), thus it can be regarded as an urban background site. The local emissions include
118 diffuse urban traffic exhaust, household/residential emissions and limited industrial sources together
119 with some off-road transport (diesel rail, shipping and airplane emissions). Experimental data for 6 full-
120 year-long time intervals, i.e. from 3 November 2008 to 2 November 2009, from 13 November 2013 to
121 12 November 2014, from 13 November 2014 to 12 November 2015, from 13 November 2015 to 12
122 November 2016, from 28 January 2017 to 27 January 2018 and from 28 January 2018 to 27 January
123 2019 were available for this single site. A decennial time interval from 03 November 2008 to 02
124 November 2018 was considered in the statistical analysis. Local time (LT=UTC+1 or daylight-saving
125 time, UTC+2) was chosen as the time base of the data processing because the ordinary daily activities
126 of inhabitants substantially influence the atmospheric concentrations and several processes in cities
127 (Salma et al., 2014).

128 The major aerosol measuring system was a flow-switching type differential mobility particle sizer
129 (DMPS, Alto et al., 2001). It records particle number concentrations in an electrical mobility diameter
130 range from 6 to 1000 nm in the dry state of particles (with a relative humidity of $RH < 30\%$) in 30
131 channels (Salma et al., 2011). The measuring system was updated twice; in spring 2013 and winter 2016.
132 Its major parts including a differential mobility analyser (DMA, Hauke-type with a length of 28 cm) and
133 a condensation particle counter (CPC, TSI model 3775) remained, however, unchanged. They were
134 cleaned and serviced. The diameter resolution of the DMA was also calibrated during the updates.
135 Several data validation or comparative exercises were realised over the years; the most extensive inter-
136 comparison was realised in summer 2015 and autumn 2019. First, the measured data by the CPC
137 deployed in the DMPS system were compared to that of an identical stand-alone CPC operated in
138 parallel. The agreement between the instruments was in accordance with the nominal specification of
139 CPCs. As the next step, the integrated concentrations obtained from the size-resolved DMPS data were
140 compared to the concentrations measured directly by the stand-alone CPC. The two instruments were

141 again operated in parallel. The median CPC/DMPS ratio was utilised as correction factor for particle
142 diffusion losses in the DMPS system (Salma et al., 2016a). The time resolution of the DMPS
143 measurements was approximately 10 min in the year 2008–2009 and it was 8 min from 13 November
144 2013 on. The sampling inlet was installed at a height of 12.5 m above the street level. There was no
145 upper-size cut-off inlet applied to the sampling line, and a rain shield and insect net were only adopted.
146 The measurements were performed according to the international technical standard (Wiedensohler et
147 al., 2012).

148 Meteorological data for air temperature (T), relative humidity (RH), wind speed (WS), wind direction
149 and atmospheric pressure (p) were obtained from a measurement station of the Hungarian
150 Meteorological Service (HMS) operated in a distance of ca. 70 m from the BpART laboratory by
151 standardised methods (Vaisala HMP45D humidity and temperature probe, Vaisala WAV15A
152 anemometer, Vaisala pressure, all Finland) with a time resolution of 10 min. Global solar radiation
153 (GRad) data were measured by a CMP11 pyranometer (Kipp and Zonnen, The Netherlands) at another
154 station of the HMS situated in 10 km in Eastern direction with a time resolution of 1 h. Concentrations
155 of pollutants SO₂, CO, NO, NO_x, O₃, and PM₁₀ mass were acquired from a measurement station of the
156 National Air Quality Network in Budapest in Széna Square, which is located in the upwind prevailing
157 wind direction in a distance of 4.5 km from the BpART laboratory. This station ordinarily measures the
158 smallest levels of the criteria air pollutants among the four monitoring stations located in the city centre.
159 It can, therefore, be considered to represent the air pollution in between the urban background and street
160 level/kerbside site. They are measured by UV fluorescence (Ysselbach 43C), IR absorption (Ysselbach
161 48C), chemiluminescence (Thermo 42C), UV absorption (Ysselbach 49C) and beta-ray attenuation
162 (Thermo 5014I) methods, respectively with a time resolution of 1 h.

163 The availability of the DMPS data over the six one-year-long time intervals were 95, 99, 95, 73, 99 and
164 90%, respectively. The meteorological data were accessible in >90% of time in each year, while the
165 concentration data for key pollutants were available in >85% of the yearly time intervals.

166 **2.2 Data treatment**

167 Particle number concentrations in the diameter ranges 1) from 6 to 1000 nm (N_{6-1000}), 2) from 6 to 100
168 nm (N_{6-100}), 3) from 25 to 100 nm (N_{25-100}) and 4) from 100 to 1000 nm ($N_{100-1000}$) were calculated from
169 the measured and inverted DMPS data. The size ranges were selected to represent 1) the total particles,
170 2) UF particles, 3) UF particles emitted mainly from incomplete combustion (and partially grown by
171 condensation; this size ranges is dominated by primary particles in cities in most of the time) and 4)
172 physically and chemically aged particles which usually represent larger spatial extent, respectively
173 (Salma et al., 2014, 2017).

174 Condensation sink (CS) for vapour molecules onto the surface of existing aerosol particles was
 175 calculated for discrete size distributions (Kulmala et al., 2001, 2012; Dal Maso et al., 2002, 2005). Dry
 176 particle diameters were considered in the calculations and condensing vapour was assumed to have
 177 sulphuric acid properties.

178 One of the key components for NPF events is the gas-phase H_2SO_4 (Sipilä et al., 2010; Sihto et al.,
 179 2011). It is challenging to measure its atmospheric concentration and, therefore, the experimental data
 180 for long time intervals are rare. The relative effects of gas-phase H_2SO_4 are, however, often estimated
 181 by deriving its proxy value. In this study, the H_2SO_4 proxy was calculated according to Mikkonen et al.
 182 (2011b), where the best proxy was based on GRad, SO_2 concentration, RH and CS. The proxy is defined
 183 for $\text{GRad} > 10 \text{ W m}^{-2}$. Other widely used proxy was introduced by Petäjä et al. (2009), but that was
 184 created for clean boreal forest environment. The most recent proxy from Dada et al. (2020) is currently
 185 under review and has not been tested against the proxy used here. All experimental data were used with
 186 their maximum time resolution.

187 The influence of large-scale weather types was considered on a daily basis by including codes for macro-
 188 circulation patterns (MCPs) invented specifically for the Carpathian Basin (Péczely, 1957; Károssy,
 189 2016). The classification is based on the extension and development of cyclones and anticyclones
 190 relative to the Carpathian Basin via the daily sea-level pressure maps constructed for 00:00 UTC in the
 191 North-Atlantic–European region. Thus defined MCP was assigned to the following day in the data.
 192 Basic information on the MCPs are summarised in Table 1.

193 **Table 1.** Macro-circulation patterns (Péczely codes) and their seasonal and annual occurrences in the Carpathian
 194 Basin for years 1958–2010 (Maheras et al., 2018).

No.	Code	Description	Occurrence (%)				
			Winter	Spring	Summer	Autumn	Annual
1	mCc	Cyclone with a cold front over NE Europe, N wind	7.3	11.3	12.1	8.0	9.7
2	AB	Anticyclone over the British Isles, N wind	5.6	7.1	8.6	6.4	6.9
3	CMc	Mediterranean cyclone with a cold front over S Europe, N wind	2.5	3.5	1.8	1.9	2.4
4	mCw	Mediterranean cyclone with a warm front over NE Europe, S wind	9.2	9.7	5.7	7.2	7.9
5	Ae	Anticyclone over E Europe, S wind	14.2	11.3	7.3	17.6	12.6
6	CMw	Mediterranean cyclone with a warm front over S Europe, S wind	8.9	8.7	3.7	8.3	7.4
7	zC	Highly developed cyclone over N Europe, W wind	5.0	3.2	2.7	2.9	3.5
8	Aw	Anticyclone over W Europe, W wind	13.1	11.2	20.8	12.8	14.6

9	As	Anticyclone over S Europe, W wind	7.0	4.4	2.9	5.6	4.9
10	An	Anticyclone over N Europe, E wind	10.9	12.8	11.3	10.1	11.3
11	AF	Anticyclone over Fennoscandia, E wind	2.8	5.2	5.9	3.7	4.4
12	A	Anticyclone over the Carpathian Basin, changing wind direction	11.8	7.3	13.3	13.3	11.4
13	C	Cyclone over the Carpathian Basin, changing wind direction	1.7	4.3	3.9	2.2	3.0

195

196 Each data line containing the date and time, concentrations, CS, H₂SO₄ proxy, meteorological data and
 197 MCP codes was further labelled by several indices on a daily basis. These labels served to differentiate
 198 between various environmental conditions, which can lead to substantial changes in some variables
 199 (Salma et al., 2014). The workdays were marked by label WD, while the holidays were denoted by label
 200 HD. Varying classes of NPF event days were also labelled differently. The classification was
 201 accomplished via the particle number size distribution surface plots (Dal Maso et al., 2005; refined in
 202 Németh et al., 2018 for urban sites) on a daily basis. The main classes were: NPF event days (marked
 203 by label NPF), non-event days (label NE), days with undefined character and days with missing data.
 204 The earliest estimated time of the beginning of a nucleation (t_1) was also derived (Németh and Salma,
 205 2014) and was added to the data record as a parameter. Finally, the data lines were labelled according
 206 to the actual technical status of the DMPS system. The data obtained from the beginning of the
 207 measurements to the 1st update was labelled as S1, the data derived between the 1st and 2nd updates were
 208 label as S2, and label S3 was given to the data obtained after the 2nd update.

209 **2.3 Statistical modelling**

210 Atmospheric data are usually not normally distributed, and, therefore, non-parametric methods are often
 211 used to detect their long-term trends (Asmi et al., 2013; Masiol et al., 2018). The coherent data set
 212 prepared as described in Sect. 2.2 was analysed in two ways. First, time trends for concentrations of
 213 particles and air pollutants were estimated by using a dynamic linear model (DLM) method. Secondly,
 214 the factors affecting the changes in particle concentrations were detected with a generalized linear mixed
 215 model (GLMM).

216 **2.3.1 Dynamic linear model**

217 Dynamic linear models (Durbin and Koopman, 2012; Petris et al., 2009; Laine, 2020) are state-of-the-
 218 art tools for time trend detection. The trend is seen as a statistical change in the properties of the
 219 background state of the system. Although changes in aerosol concentrations have previously been
 220 approximated with linear trends (e.g. Sun et al., 2020), this is not always the most suitable method since
 221 the processes affecting the concentrations are continuously evolving over time. Additionally, time series
 222 of atmospheric measurements can include multiple time-dependent cycles (e.g. seasonal and diurnal
 223 cycles) which are typically non-stationary – meaning that their distributional properties change over

224 time. The DLM approach effectively decomposes the data series into basic components such as level,
 225 trend, seasonality and effect of external forcing by describing statistically the underlying structure of the
 226 process that generated the measured data. All these components are defined by Gaussian distributions,
 227 and they are allowed to vary in time, and the significance and magnitude of this variation can also be
 228 modelled and estimated. In the basic setup of DLM, the sign or the magnitude of the trend is not defined
 229 in advance by the model formulation but estimated from the data. The method can detect and quantify
 230 trends, but the explanations for the observed changes is provided by the user. Nevertheless, it determines
 231 if the observations are consistent with the selected model. We used the DLM to explain variability in
 232 the particle concentration time series using following components: locally linear mean level, trend,
 233 seasonal effect, autoregressive component and noise. The autoregressive component is added to the
 234 model in order to take account the autocorrelation in the data, i.e. the correlation between subsequent
 235 observations. Here it refers to first order autoregressive model (AR(1)). The evolution of the investigated
 236 concentrations – after the seasonal and noise components were filtered out – is modelled by using the
 237 smoothed mean level. Here, the change in the mean level is the trend of the variable. The statistical
 238 model can be described by the following equations (Mikkonen et al., 2015):

$$239 \quad y_t = \mu_t + \gamma_t + \eta_t + \varepsilon_{obs}, \varepsilon_{obs} \sim N(0, \sigma_t^2), \quad (1)$$

$$240 \quad \mu_t = \mu_{t-1} + \alpha_t + \varepsilon_{level}, \varepsilon_{level} \sim N(0, \sigma_{level}^2), \quad (2)$$

$$241 \quad \alpha_t = \alpha_{t-1} + \varepsilon_{trend}, \varepsilon_{trend} \sim N(0, \sigma_{trend}^2), \quad (3)$$

$$242 \quad \eta_t = \rho\eta_{t-1} + \varepsilon_{AR}, \varepsilon_{AR} \sim N(0, \sigma_{AR}^2), \quad (4)$$

243 where y_t is the investigated concentration at time t , μ_t is the mean level and α_t is the change in the level
 244 from time $t-1$ to time t , γ_t is the seasonal component, η_t is an autoregressive error component and ρ is
 245 the coefficient for autoregressive component, here fixed to $\rho = 0.6$. Here, this latter level is fixed. The
 246 Gaussian stochastic ε terms are used for the observation uncertainty and for random dynamics of the
 247 level and the trend. The seasonal component γ_t contains dummy variables for each month, so it has a
 248 different value for each month with a condition that 12 consecutive months sum to zero. More detailed
 249 description on how the model is written through state space equation can be found in Mikkonen et al.
 250 (2015).

251 **2.3.2 Generalized linear mixed model**

252 Linear mixed models (McCulloch et al., 2008) belong to the family of models that combine several
 253 different kinds of models used in multivariate analysis when the data do not fulfil the standard
 254 independency and homogeneity assumptions. This is the normal case with atmospheric and
 255 climatological measured variables (e.g. Mikkonen et al., 2011a). The main goal of the mixed models is
 256 to estimate not only the mean of the measured response variable but also the variance-covariance

257 structure of the data, which makes the model more valid for complex atmospheric data. In addition,
 258 modelling the (co)variances of the variables reduces the bias of the estimates, and prevents
 259 autocorrelation of the residuals. The model is constructed from general linear model, written in matrix
 260 format as $y = \mathbf{X}\boldsymbol{\beta} + \boldsymbol{\varepsilon}$, by adding a so-called random component (denoted $\mathbf{Z}\mathbf{u}$) to the model, thus the model
 261 is given by $y = \mathbf{X}\boldsymbol{\beta} + \mathbf{Z}\mathbf{u} + \boldsymbol{\varepsilon}$. Here, if we let n equal to number of observations, p equal to number of fixed
 262 parameters and q equal to number of random parameters in the model, \mathbf{y} is the $(n \times 1)$ vector of
 263 measurements of the variable of interest, $\boldsymbol{\beta}$ denotes the unknown $(p \times 1)$ vector of intercept and slope
 264 estimates of the model, \mathbf{X} is the $(n \times p)$ matrix of observations from predictor variables and $\boldsymbol{\varepsilon}$ contains
 265 the residuals of the model. In the random part, \mathbf{Z} is the $(n \times q)$ design matrix for the $(q \times 1)$ vector of
 266 random covariates \mathbf{u} with a q -dimensional normal distribution. With adequate choices of the matrix \mathbf{Z} ,
 267 different covariance structures $\text{Cov}(\mathbf{u}) = \mathbf{G}$ and $\text{Cov}(\boldsymbol{\varepsilon}) = \mathbf{R}$ can be defined and fitted. Successful modelling
 268 of variances and covariances of the observations provides valid statistical inference for the fixed effects
 269 $\boldsymbol{\beta}$ of the mixed model. In contrast to general linear models, the error terms $\boldsymbol{\varepsilon}$ can be correlated, which
 270 makes the modelling more robust. It follows from this that the distribution of observations can be
 271 described by a normal distribution with the expectation of $\bar{\mathbf{X}}$ and covariance matrix \mathbf{V} , which is given
 272 by $\mathbf{V} = \mathbf{Z}\mathbf{G}\mathbf{Z}' + \mathbf{R}$. With GLMM, it is possible to reliably detect the factors which affect particle number
 273 concentrations or which act as indicators for their different sources. The model can be expressed in a
 274 mathematical form as (Mikkonen et al., 2011a):

$$\begin{aligned}
 275 \quad N_{Di} &= (\beta_0 + \beta_{setup} + u_m) + \alpha_d + (\beta_{wd} \cdot \beta_E) \cdot X_{Ti} + (\beta_1 + v_{1m}) \cdot SO_{2,i} + (\beta_2 + v_{2m}) \cdot NO_{2,i} + \\
 276 \quad &(\beta_3 + v_{3m}) \cdot O_{3,i} + \beta_4 \cdot GRad_i + \beta_5 \cdot RH_i + \beta_6 \cdot MCP_i, \quad (5)
 \end{aligned}$$

277 where N_{Di} is the number concentration in selected size range in time i , β_0 is a model intercept, β_{setup} is
 278 a correction term for changes in the measurement system due to two major upgrades, u_m is vector of
 279 random intercepts different for each month, α_d is average change of N_{Di} per day (i.e. slope of trend),
 280 β_{wd} and β_E are coefficients for workday and NPF event day, respectively, and X_{Ti} is the corresponding
 281 vector showing the type of the day (in both means: WD/HD and E/NE) in time i , $\beta_1 - \beta_5$ are fixed
 282 coefficients for SO_2 , NO_2 , O_3 , $GRad$ and RH , respectively, β_6 is the (13×1) vector of coefficients for
 283 different macro-circular patterns (MCP) indicating the characteristic level of number concentration
 284 during each MCP type, which are treated here as categorical variable, and v_m are the random, month
 285 specific slopes for SO_2 , NO_2 , O_3 and $GRad$. The coefficients of the model can be interpreted in a similar
 286 manner as multivariate regression or general linear models, just with an addition of month-specific
 287 effects for given variables.

288 3 Results and discussion

289 Annual insolation (Q), which expresses the total energy density at a receptor site, was derived from the
 290 individual hourly mean $\text{GRad}_{i,j}$ data, where index i represents the hour of day (from 0 to 23) and index
 291 j stands for the day of year (from 1 to 365) as $Q = 3.6 \times 10^{-6} \times \sum_{i,j} \text{GRad}_{i,j}$. The dimensions of the
 292 individual $\text{GRad}_{i,j}$ data and Q are W m^{-2} and $\text{GJ m}^{-2} \text{y}^{-1}$, respectively. The few randomly missing
 293 datapoints were interpolated linearly. Since the major sources of particles in cities include road vehicles
 294 and atmospheric nucleation, we added some indicative data on these specific sources as well. The
 295 median particle number concentrations are basically in line with many other comparable cities in the
 296 world (e.g. Kerminen et al., 2018; Masiol et al., 2018). They indicate a decreasing change (except for
 297 $N_{100-1000}$) over the years 2008–2018. At the same time, the annual averages of the other concentrations,
 298 meteorological data and auxiliary variables did not change substantially. Annual mean relative
 299 occurrence frequency of NPF events stayed almost constant with a mean and SD of $(20 \pm 4)\%$, except for
 300 the measurement year 2015–2016 when it was unusually small. It is worth adding that the NPF increases
 301 the existing particle number concentrations in Budapest by a factor of approximately 2 on event days
 302 (Salma et al., 2017). The annual medians for the particle formation rate and particle growth rate also
 303 stayed constant and seemingly varied only as fluctuations within ca. $\pm 20\%$ and $\pm 8\%$, respectively. The
 304 number of passenger cars was registered in Budapest remained constant within $\pm 5\%$, while the share of
 305 the diesel-powered passenger cars increased modestly by a rate of approximately 12% from 2008 to
 306 2018 (KSH, 2019). The number (ca. 4000) of buses registered in Budapest and the share (98%) of the
 307 diesel-power buses on the national bus fleet remained constant.

308 **Table 2.** Annual medians of particle number concentrations in the diameter ranges from 6 to 1000 nm (N_{6-1000}),
 309 from 6 to 100 nm (N_{6-100}), from 25 to 100 nm (N_{25-100}) and from 100 to 1000 nm ($N_{100-1000}$), concentrations of SO_2 ,
 310 CO, NO, NO_x , O_3 , PM_{10} mass, annual means of air temperature (T), relative humidity (RH), wind speed (WS),
 311 atmospheric pressure (P) and annual insolation (Q), annual mean relative occurrence frequency of nucleation
 312 (f_{NPF}), annual median formation rate of particles with a diameter of 6 nm (J_6), annual median growth rate of
 313 particles with a diameter of 10 nm (GR_{10} ; for the rates, see Salma and Németh, 2019), number of passenger cars
 314 registered in Budapest (Cars), the mean age and the share of diesel-powered vehicles (Diesel) separately for the 1-
 315 year-long measurement time intervals.

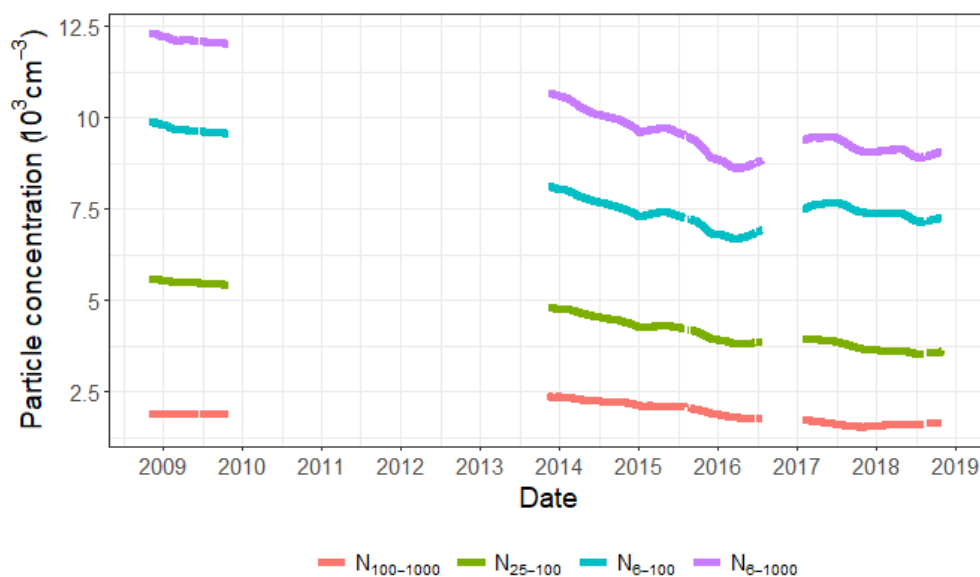
Variable	Unit	2008–2009	2013–2014	2014–2015	2015–2016	2017–2018	2018–2019
N_{6-1000}	10^3 cm^{-3}	11.5	9.7	9.3	7.5	8.6	8.3
N_{6-100}	10^3 cm^{-3}	9.1	7.2	6.9	5.7	6.8	6.5
N_{25-100}	10^3 cm^{-3}	5.1	4.3	4.1	3.3	3.6	3.2
$N_{100-1000}$	10^3 cm^{-3}	1.79	2.2	2.0	1.56	1.49	1.53
SO_2	$\mu\text{g m}^{-3}$	5.0	4.8	4.6	4.8	4.5	5.2
CO	$\mu\text{g m}^{-3}$	547	488	577	513	534	624
NO	$\mu\text{g m}^{-3}$	13.3	19.2	23	17.6	20	17.0
NO_x	$\mu\text{g m}^{-3}$	58	80	89	72	79	73
O_3	$\mu\text{g m}^{-3}$	23	14.8	19.6	25	20	21

PM ₁₀	µg m ⁻³	33	31	39	29	28	36
<i>T</i>	°C	12.0	13.2	13.2	12.9	13.2	13.3
RH	%	64	69	64	69	63	67
WS	m s ⁻¹	2.5	2.6	2.8	2.7	2.9	2.5
<i>P</i>	hPa	1001	1003	1005	1004	1004	1004
<i>Q</i>	GJ m ⁻² y ⁻¹	4.45	4.39	4.58	4.52	4.77	4.66
<i>f</i> _{NPF}	%	24	20	23	13.0	23	20
<i>J</i> ₆	cm ⁻³ s ⁻¹	4.2	3.5	4.4	4.6	6.3	4.6
GR ₁₀	nm h ⁻¹	7.6	6.6	6.5	8.0	7.5	7.0
Cars*	10 ³ pcs	582	573	584	597	634	659
Age*	y	10.8	13.0	13.4	13.7	14.1	14.2
Diesel*	%	20	24	26	28	29	n.a.

316 * Status at the end of years 2009, 2013, 2014, 2015, 2017 and 2018, respectively.
 317 n.a.: not yet available.

318 3.1 Decennial time scale

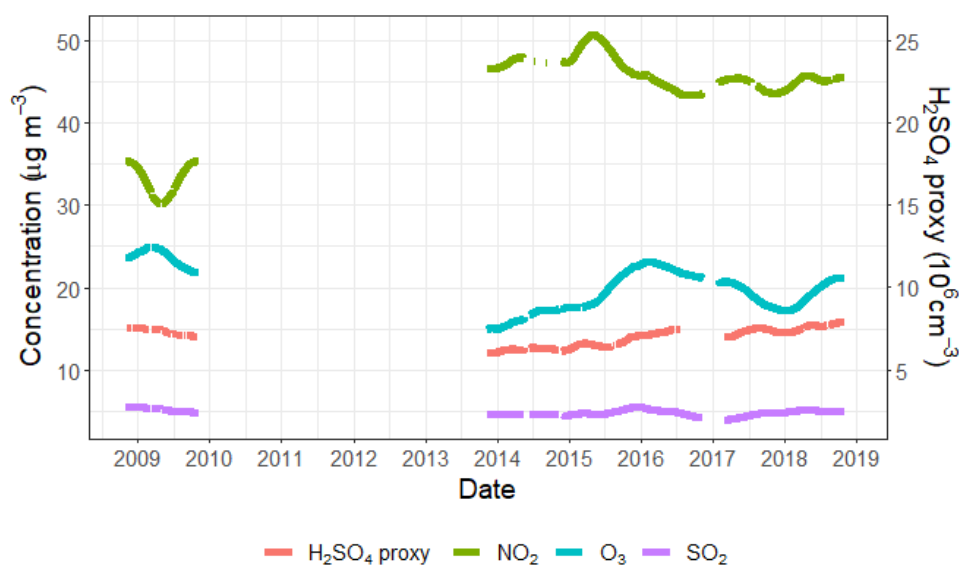
319 Overall statistical time trends for particle number concentrations in various size fractions obtained by
 320 the DLM are displayed in Figure 1. The curves confirm that the N_{6-1000} , N_{6-100} and N_{25-100} indeed
 321 decreased in Budapest between 2008 and 2018, while the change in $N_{100-1000}$ was not significant. The
 322 decline mostly took place in a monotonical manner except for perhaps the interval of summer 2016–
 323 spring 2017, when some partial/local increase could be realised for N_{6-1000} and N_{6-100} .



324 **Figure 1.** Statistical time trends of particle number concentrations in the diameter ranges from 6 to 1000 nm (N_{6-1000}),
 325 from 6 to 100 nm (N_{6-100}), from 25 to 100 nm (N_{25-100}) and from 100 to 1000 nm ($N_{100-1000}$) derived by DLM
 326 over a decennial interval.

327 There are several important sources, sinks and atmospheric transformation processes including
 328 environmental conditions which can influence the atmospheric concentrations. The major sources
 329 include both high-temperature emissions and NPF events as discussed in Sect. 1. The latter source is
 330 affected by concentrations of precursor and other trace gases, meteorological properties for
 331 photochemical reactions, and the interactions among gas-phase chemical species of different origin/type

332 with respect the formation yield of condensing vapours (Kulmala et al., 2014; McFiggans et al., 2019).
 333 The air pollutants listed in Table 2 and gas-phase H₂SO₄ proxy – which are known or expected to affect
 334 particle number concentrations – did not exhibit decreasing statistical trend between 2008 and 2018
 335 (Fig. 2). On one hand, this decoupling suggests that the causes of the decrease in particle number
 336 concentrations are not primarily related to meteorological conditions because they would jointly affect
 337 the gas concentrations as well (if their sources are more-or-less constant over a certain time interval).
 338 On the other hand, the constant gas concentrations suggest that the decreasing trend in particles does not
 339 seem to be related to the major precursors or interacting gaseous chemical species (such as SO₂, H₂SO₄
 340 or NO₂).



341 **Figure 2.** Statistical time trends of gas-phase H₂SO₄ proxy, SO₂, O₃ and NO₂ derived by DLM over the decennial
 342 interval.

343 As far as the meteorological conditions are concerned, some of them such as WS, atmospheric boundary
 344 mixing layer height and *T* have previously been shown to influence the temporal variation of aerosol
 345 particles (e.g. Birmili et al., 2001; Mikkonen et al., 2011a). The annual means of possibly relevant
 346 properties and parameters in Table 2 – except for the particle number concentrations (which are under
 347 the investigation) and the fraction of diesel cars – did not show any obvious dependency; they virtually
 348 stayed constant over the years of interest. The possible effect of different weather conditions on the
 349 concentrations are studied separately by the GLMM and are discussed in Sect. 3.2.2. There were also
 350 no substantial and extensive urban constructions in the area (which could influence the urban air flow)
 351 nor larger systematic changes in the traffic circulation around the sampling site in the time interval
 352 considered. Therefore, the decline in the particle number concentrations can likely be interpreted as a
 353 consequence of the decreased anthropogenic particulate emissions in Budapest. The related source
 354 sectors can include vehicular road traffic and household heating/cooking. The decline happened at an
 355 increasing share of the diesel passenger cars and straitened emission control on (diesel) vehicles, as e.g.

356 Platt et al. (2017) and Wihersaari et al. (2020) showed that modern diesel engines have lower particle
 357 emissions than gasoline engines.

358 The average decrease rates of particle number concentrations as derived from both the DLM and GLMM
 359 statistical approaches are summarised in Table 3. The rates are shown as obtained from the models and
 360 scaled for the 10-year measurement interval to ensure the comparability of the slopes. The relative mean
 361 changes in % per year were expressed with respect to the starting value (mean of the first year). There
 362 are some differences between the corresponding results of the two models, which were caused by
 363 standardising the concentrations with the predictors in the models and by handling the upgrades of
 364 measurement setup differently. The changes in all size fractions were on the same level and only minor
 365 differences could be seen. As the estimates always contain some uncertainty, these differences are not
 366 considered as statistically significant. The largest difference between the two models was observed for
 367 $N_{100-1000}$ (which had the lowest absolute concentrations). One possible cause for this might be that
 368 GLMM standardises the results for variables indicating anthropogenic emissions and thus the size
 369 fraction that is the most sensitive for the emissions has the strongest effect. Considering all these, the
 370 rates from the two statistical models agree well. Furthermore, the rates for N_{6-1000} and N_{6-100} were
 371 identical. This is explained by the fact that these two size fractions are strongly connected; the typical
 372 N_{6-100}/N_{6-1000} mean ratio in central Budapest is 75–80% (Salma and Németh, 2019). Small difference
 373 was also seen for N_{25-100} . In urban areas, this size fraction is mainly composed of particles from high-
 374 temperature emission sources. The source types responsible for the observed decline are further
 375 discussed in Sect. 3.2.1.

376 **Table 3.** Decrease rates of particle number concentrations in the diameter ranges from 6 to 1000 nm, from 6 to
 377 100 nm, from 25 to 100 nm and from 100 to 1000 nm obtained by the dynamic linear model and generalized linear
 378 mixed model as a mean absolute change per year during the 10-year measurement interval and as a relative mean
 379 change per year with respect to the mean value of the first year.

Size fraction (nm)	Dynamic linear model		Generalized linear mixed model	
	Mean change/year (cm ⁻³)	Relative mean change (%/year)	Mean change/year (cm ⁻³)	Relative mean change (%/year)
6–1000	–510	–4	–660	–5
6–100	–400	–4	–480	–5
25–100	–310	–6	–360	–5
100–1000	–50	–3	–180	–8

380
 381 Our results concerning the decennial change rates (and our conclusions with regard to their causes
 382 mainly discussed in Sect. 3.2.1) are comparable and are in line with some other very recent studies. Sun
 383 et al. (2020) investigated the statistical concentration trends in particle numbers (and equivalent black
 384 carbon mass) at multiple urban, rural or background sites within the German Ultrafine Aerosol Network.

385 Decreasing annual slopes of $-(7.0-1.7)\%$ were obtained for several size fractions (which are different
386 from our intervals), and the most likely factors for the decreasing trends were assigned to declining
387 anthropogenic emissions due to emission mitigation policies of the EU. Masiol et al. (2018) evaluated
388 statistical time trends of particle number concentrations in various size fractions (which are different
389 again from the previous and present studies) in Rochester, NY, USA, and obtained a typical decline rate
390 of -4.6% per year for total particles. These outcomes and our data as well seem to be different from the
391 results obtained by Saha et al. (2018) in the urban Pittsburgh, PA, USA by comparing two intervals of
392 2001–2002 and 2016–2017. It should be mentioned that in the latter research, the experimental setup
393 for measuring particle number size distributions had a lower diameter limit of detection at 11 nm, some
394 methodological approaches (e.g. classification of events) were different from ours and that the time trend
395 was not derived by statistical modelling. The authors concluded that both the frequency of NPF events
396 and their dynamic properties were reduced by (40–50)% over the past 15 years, resulting in ca. 48%
397 reduction of UF concentrations. The changes were attributed to dramatic reductions in SO_2 emissions in
398 the larger region.

399 **3.2 Diurnal time scale**

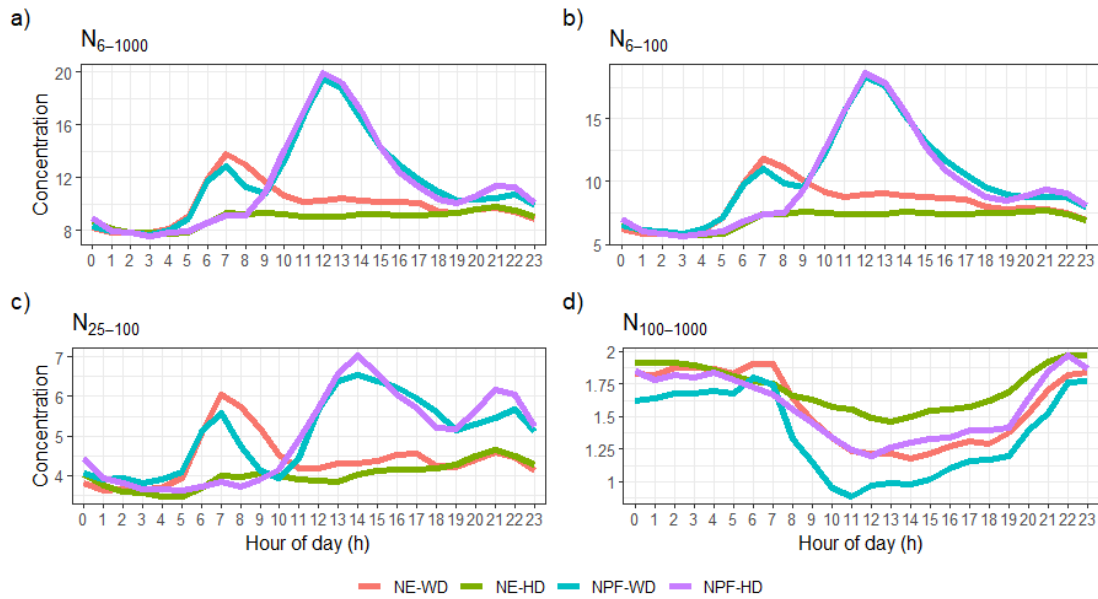
400 Diurnal statistical patterns of the particle number concentrations in different size fractions were
401 predicted by the GLMM considering the following variables: GRad, RH, concentrations of SO_2 , NO_2 ,
402 O_3 , and labels for workdays/holidays, for NPF event days/non-event days and for MCP codes. The initial
403 screening for possible prediction variables was done in earlier papers. Studies such as Hyvönen et al.
404 (2005), Mikkonen et al. (2006) and Nieminen et al. (2014) suggested that meteorological and trace gas
405 variables affect NPF. Furthermore, e.g. Mikkonen et al. (2011a), Guo et al. (2012) and Zaidan et al.
406 (2018) studied the factors which influence the growth of freshly formed particles as well as the
407 concentrations of particles in larger size fractions and specified the possible predictors. All variables
408 found in these screenings and measured at our site were tested one-by-one in the GLMM model in a
409 stepwise manner. In each step, the significance of the added or removed variable was investigated by a
410 likelihood ratio test (e.g. Pinheiro and Bates, 2000) until the final model shown in Eq. 4 was formed.
411 The effect of the H_2SO_4 proxy was also tested, and the results for the daytime concentrations were
412 similar to those obtained with the selection of variables above. The modelling results for night-time
413 were, however, biased since the proxy is defined for $\text{GRad} > 10 \text{ W m}^{-2}$, and, therefore, we decided not to
414 include the proxy into the final model.

415 **3.2.1 Diurnal statistical patterns**

416 Modelled diurnal pattern of particle number concentrations for event days on workdays, event days on
417 holidays, non-event days on workdays and non-event days on holidays separately for different size
418 fractions are shown in Fig. 3. The curves on Fig. 3a–c resemble tendentious variations, which can be
419 associated with typical diurnal activity–time pattern of inhabitants in cities, particularly with road traffic.

420 They are also perfectly in line with the mean diurnal tendencies of experimentally determined
421 concentrations in central Budapest (Salma et al., 2014; 2017) and are consistent with the time variations
422 in many other European cities (Hussein et al., 2004; Aalto et al., 2005; Moore et al., 2007; Avino et al.,
423 2011; Dall'Osto et al., 2013).

424 In the statistical diurnal patterns of UF particles (Fig. 3b), there is a huge peak from late morning to late
425 afternoon on event days. This is unambiguously caused by NPF and growth process. The peaks on
426 workdays and holidays are rather similar to each other in the position, shape and magnitude (area), which
427 means that the dynamics and timing of NPF events in general are not substantially influenced by
428 anthropogenic activities, which are more intensive on workdays than on holidays. It is worth mentioning
429 that the overall contribution of the NPF to particle number concentrations is less than what is seemingly
430 indicated by the diurnal patterns alone since NPF events occur on approximately 20% of days (Table 2).
431 Emissions from vehicular road traffic is represented by a notable peak during the morning rush hours
432 (between 05:30 and 08:30) on workdays. It is noted that the boundary layer mixing height is usually
433 increased during this interval because of the increasing solar radiation intensity and mixing intensity.
434 Another peak occurred around 21:00, thus later than the afternoon rush, which usually happens between
435 16:30 and 18:30. Under strong anti-cyclonic conditions, the evolution of the boundary layer mixing
436 height and mixing intensity can decrease the concentration levels in the afternoons until sunset, and this
437 can compensate the increased intensity of emissions. This all means that the afternoon peak is realised
438 in a fuzzy manner since it is more influenced by local meteorology than by vehicular emissions. The
439 effect of residential heating and combustion activities at evenings can also play a role. It is worth noting
440 that the early-morning rush-hour peak on event days was smaller than on non-event days, which agrees
441 with our earlier observation derived directly from experimental data (Salma et al., 2017) and is in line
442 with the overall picture on urban NPF events (Zhang et al., 2015; Kulmala et al., 2017). On holidays,
443 the modelled diurnal variation for non-event days contained an increasing part in the morning to a
444 modest concentration level, which remains fairly constant over the daytime. This is explained by the
445 differences in daily activities of citizens on workdays and holidays as far as both their intensity and
446 timing are concerned.



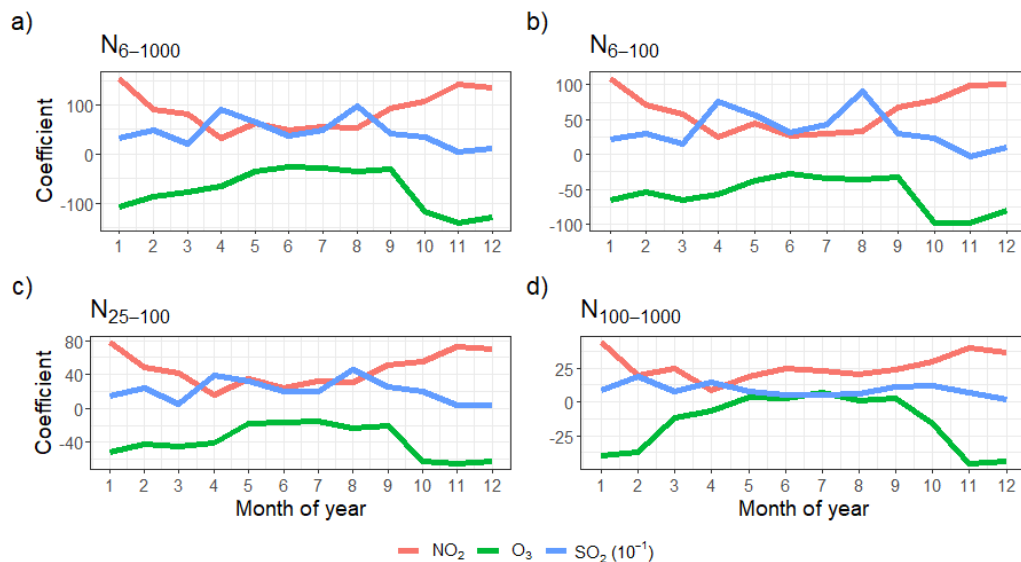
447
 448 **Figure 3.** Diurnal patterns of particle number concentrations in the diameter ranges from 6 to 1000 nm (N_{6-1000}),
 449 from 6 to 100 nm (N_{6-100}), from 25 to 100 nm (N_{25-100}) and from 100 to 1000 nm ($N_{100-1000}$) in units of 10^3 cm^{-3} .
 450 Red: non-event on workdays, green: non-event on holidays, cyan: event on workdays, purple: event on holidays.

451 The statistical diurnal patterns of N_{6-1000} trends (Fig. 3a) were very similar or analogous to those of the
 452 N_{6-100} . These two size fractions are strongly connected with each other as explained in Sect. 3.1. The
 453 diurnal curves for N_{25-100} (Fig. 3c) were also similar to the previous corresponding curves as far as the
 454 character and shape are concerned, while there were also evident differences between their relative
 455 structures. The peaks for the early morning and late afternoon rush hours were relatively larger than in
 456 the trends of 6–100- or 6–1000-nm size fractions due to the higher contribution of primary particles
 457 from high temperature sources in this size fraction. New particle formation generally occurs on days
 458 when N_{25-100} are smaller before the event onset (between 08:00 and 11:00). The maximum of the peaks
 459 associated with NPF events in Fig. 3a and b – which is between 12:00 and 13:00 – was also shifted to
 460 later, i.e. to ca. 14:00 in Fig. 3c. This can be explained by the time needed for freshly nucleated particles
 461 to reach the diameter range >25 nm.

462 The statistical diurnal patterns for $N_{100-1000}$ seem very different from the smaller size ranges. First, their
 463 time variations were rather small in comparison to the other size fractions. On workdays, they only
 464 showed a modest elevation from 06:00 to 08:00 (morning rush hours), which is mainly caused by
 465 resuspension of road/surface dust particles by moving vehicles or by emissions of coarse particles from
 466 material wear. This morning peak was even missing on holidays, but another small and broad elevation
 467 showed up from 21:00 to 22:00. This and the overall changes during the daylight time are primarily
 468 related to the daily cycling of local meteorological conditions, in particular of boundary layer mixing
 469 height under stable anti-cyclonic weather conditions, outlined above.

470 **3.2.2 Effects of variables**

471 Monthly mean coefficients (mean v_m slopes in Eq. 4) of NO₂, O₃ and SO₂ derived by GLMM, which
 472 express their partial effects on particle number concentrations are shown in Fig. 4 for different size
 473 fractions.



474
 475 **Figure 4.** Distribution of monthly mean coefficients (which are proportional to the partial effects) for NO₂, O₃ and
 476 SO₂ on particle number concentrations separately in the diameter ranges from 6 to 1000 nm (N_{6-1000}), from 6 to
 477 100 nm (N_{6-100}), from 25 to 100 nm (N_{25-100}) and from 100 to 1000 nm ($N_{100-1000}$).

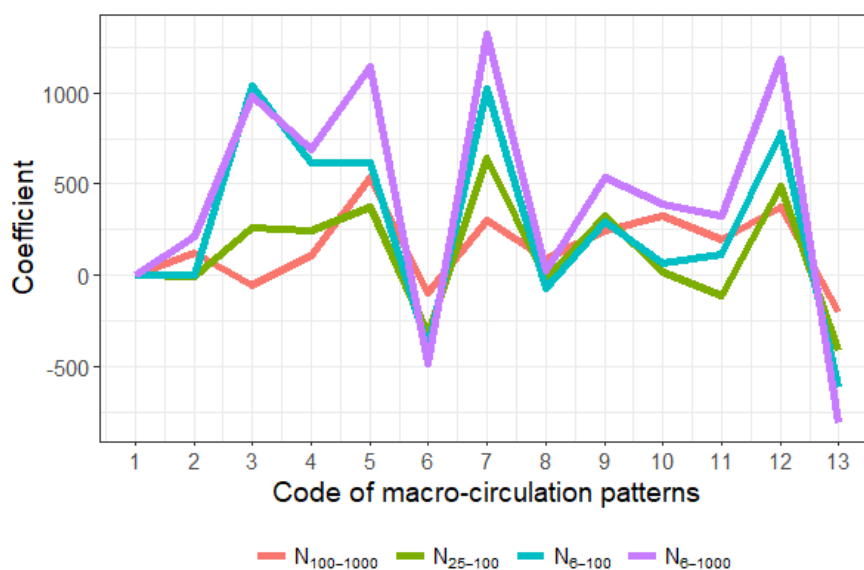
478 The coefficients of SO₂ and NO₂ are positive, while O₃ seems to have a decreasing effect on particle
 479 number concentrations. The coefficients all have seasonal patterns, which means that the magnitude of
 480 their effect on particle concentrations are of different magnitude in different months. This means for
 481 example that 1 $\mu\text{g m}^{-3}$ increase in NO₂ concentration increases N_{6-1000} concentration in January by 154
 482 m^{-3} but in June by 50 m^{-3} . This could, however, be partly caused by annual changes of boundary layer
 483 mixing height or some other variable affecting particle concentrations, and correlating with these, but
 484 not measured at the site. The boundary layer mixing height tends to be smaller in Budapest in winter
 485 than in the other seasons (Salma et al., 2011), which ordinarily results in higher atmospheric
 486 concentrations at steady-state absolute amounts of chemical species. The coefficients of NO₂ on N_{6-1000} ,
 487 N_{6-100} and N_{25-100} were higher in winter. This may indicate that large fractions of particles in these three
 488 size fractions originate from residential heating and NO₂ acts as an indicator for this source. Another
 489 major source of NO₂ and primary particles is the road traffic, but this does not show seasonal variation
 490 in Budapest. The seasonal effect of NO₂ on chemically aged, regional type particles ($N_{100-1000}$) may not
 491 be significant.

492 The partial effect of O₃ on N_{6-1000} , N_{6-100} and N_{25-100} was weaker in summer, late spring and early autumn.
 493 This interval coincides with relatively large O₃ concentrations in the area. Ozone has a strong seasonal
 494 variation (as shown in Fig. S1 in the Supplement). The negative correlation between O₃ concentration

495 and its effect on particle concentrations need further clarification since O_3 participates in a large variety
 496 of complex atmospheric processes and also serves as a marker for photochemical processes which
 497 influence secondary particle formation. The influence of O_3 on $N_{100-1000}$ was virtually negligible due
 498 likely to the regional character of these particles (which are usually chemically aged and often represent
 499 larger spatial scale due to their larger atmospheric residence time) similarly to NO_2 . In addition, O_3
 500 might act as an indicator of particulate pollution from traffic, power plants and other anthropogenic
 501 sources. Then more ozone would indicate higher number of larger particles and due to coagulation less
 502 smaller particles.

503 The partial effects of SO_2 on the particle number concentrations were the largest of the three gases
 504 considered. In the N_{6-1000} , N_{6-100} and N_{25-100} , two peaks appeared, one in spring and another one in late
 505 summer. This shape is in line with the average distribution of the monthly mean relative NPF occurrence
 506 frequency in Budapest (Salma and Németh, 2019). The latter distribution consists of an absolute and a
 507 local minimum in January (with a monthly mean occurrence frequency of 5.9%) and in August (17.0%),
 508 respectively, and an absolute and a local maximum in April (41%) and in September with (26%),
 509 respectively. The distribution of the SO_2 coefficient suggests and confirms that SO_2 , via NPF events
 510 contribute in a substantial extent to the particle number concentrations in cities. The influence of SO_2
 511 on $N_{100-1000}$ was virtually negligible due likely to the regional character of these particles similarly to the
 512 other two gases included into the model.

513 Figure 5 summarizes the effect of macro-circulation patterns on particle number concentrations in the
 514 different size fractions. It is seen that the larger regional-type particles are less affected by the MCPs
 515 than the smaller particles. The weather conditions favouring NPF events can be identified from the
 516 curves by looking at the largest coefficients for size fraction of 6–100 nm.

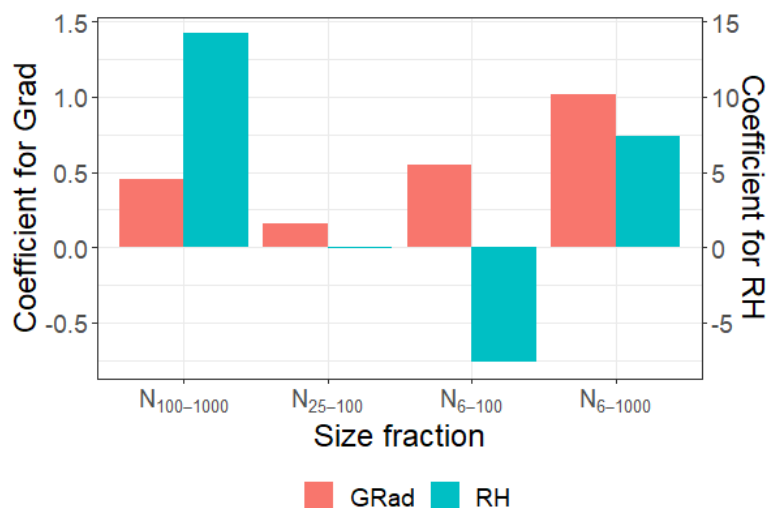


517

518 **Figure 5.** Distribution of monthly mean coefficients (which are proportional to the partial effects) for macro-
519 circulation patterns (Péczezy codes) on particle number concentrations separately in the diameter ranges from 100
520 to 1000 nm ($N_{100-1000}$), from 25 to 100 nm (N_{25-100}), from 6 to 100 nm (N_{6-100}) and from 6 to 1000 nm (N_{6-1000}).

521 It seems that the MCP no. 3 (Mediterranean cyclone with a cold front over S Europe, N wind), 7 (highly
522 developed cyclone over N Europe, W wind) and 12 (anticyclone over the Carpathian Basin, changing
523 wind direction) can represent favourable conditions for NPF events than the other MCPs. Under these
524 conditions, the weather in the area is typically windy, with average solar radiation (expect for MCP no.
525 3 in summer when it shows low daily values), with strong planetary bounding layer evolution and
526 consequently, iv) the pollutants concentrations are below the average (expect for the winter inversions
527 in MCP no. 12). The air pollution situations are better separated by MCP codes in summer than in winter.
528 The weather type classified as no. 6 (Mediterranean cyclone with a warm front over S Europe, S wind)
529 disfavour the events. Under these conditions, the weather is typically cloudy and rainy with lower than
530 average solar radiation. This situation is often associated with polluted air in Budapest. Proportions for
531 NPF days for different MCP codes, which are shown Table S1 in the Supplement, also confirm these
532 conclusions. In order to see if the decreasing concentrations are due to changes in meteorological
533 patterns, we investigated separately the occurrence of the MCP patterns during the measurement period.
534 We found no significant changes in the occurrence of the patterns and thus the decreasing particle
535 concentrations are due to something else than the meteorological patterns.

536 The coefficients for GRad and RH for different size fractions are shown in Fig. 6. It was found that these
537 variables do not have seasonal dependency, i.e. they contribute with equal strength to particle
538 concentrations throughout the year. Effect of GRad is positive for all size fractions, but it is weaker for
539 larger (regional-type or already chemically aged or processed) particles. The latter contribution could
540 be related to the bias in meteorological properties as well. The RH has negligible effect on size fraction
541 of 25–100 nm. It affects strongly and positively the largest particles, which means that the particles are
542 larger within higher humidity. This might be related to local meteorology, as higher RH probably means
543 more clouds and more clouds probably means less radiation and lower boundary layer and this could



544 cause higher particle concentration. In contrast, the effect of RH on the smallest particles was negative,
 545 which is probably caused by high RHs, which limit NPF (e.g. Hamed et al., 2011).

546 **Figure 6.** Distribution of monthly mean coefficients (which are proportional to the partial effects) for global
 547 radiation (GRad) and relative humidity (RH) separately in the diameter ranges from 100 to 1000 nm ($N_{100-1000}$),
 548 from 25 to 100 nm (N_{25-100}), from 6 to 100 nm (N_{6-100}) and from 6 to 1000 nm (N_{6-1000}).

549 3.2.3 Goodness-of-fit evaluation for GLMM

550 In order to estimate the uncertainty of the models for different size fractions, we calculated the mean
 551 absolute errors relative to the dependent variable mean, given by Willmot et al. (2009):

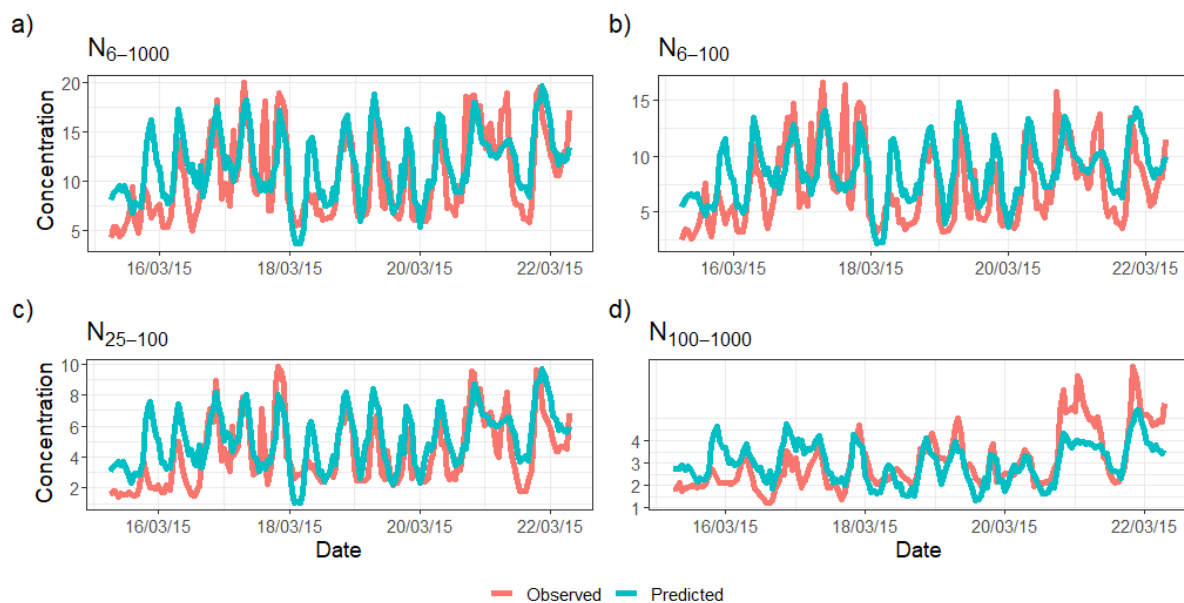
$$552 \text{Err} = (n^{-1} \sum_{i=1}^n |y_i - \hat{y}_i|) \cdot \bar{y}^{-1}, \quad (5)$$

553 where n is the number of observations, y_i are the observed particle number concentrations, \hat{y}_i are the
 554 predicted values given by the GLMM and \bar{y} is the mean of the observed values. In addition, we
 555 calculated Spearman's rank correlation coefficients between the observed and predicted values for all
 556 size fractions. Both goodness-of-fit estimates are shown in Table 4. As the relative errors for different
 557 size fractions are within a range of 0.30–0.34 and the correlations are higher than 0.70, it can be
 558 concluded that the model fitted the data with this size and measurement uncertainty well.

559
 560 **Table 4.** Goodness-of-fit estimates for GLMM as expressed by the mean absolute error relative to the dependent
 561 variable mean and by Spearman's rank correlation coefficient separately in the size fractions of 6–1000, 6–100,
 562 25–100 and 100–1000 nm.

Size fraction	Error	Correlation
6–1000	0.30	0.73
6–100	0.32	0.72
25–100	0.34	0.71
100–1000	0.34	0.73

563
 564 Figure 7 illustrates how well the GLMM model predicts the observations in all size fractions within a
 565 randomly selected period of one week in March 2015. The figure shows that the predicted values follow
 566 the observations fairly well in all size fractions. Overall, the statistical model finds the peaks of the
 567 concentration, but slightly underestimates the highest peaks and the fastest fluctuations and in some
 568 cases, overestimates the lowest concentrations.



569
 570 **Figure 7.** Observed (red line) and predicted (cyan line) time series for an illustrative example period separately in
 571 the size fractions of 6–1000, 6–100, 25–100 and 100–1000 nm.

572 4 Conclusions

573 In the present study, we determined decennial statistical time trends and diurnal statistical patterns of
 574 atmospheric particle number concentrations in various relevant size fractions in the city centre of
 575 Budapest in an interval of 2008–2018. The decennial statistical trends showed decreasing character in
 576 all applied size fractions of particle concentrations. The mean overall decrease rate was approximately
 577 –5% scaled for the 10-year measurement interval. One of the likely explanations of the decline is due to
 578 the decreased anthropogenic emissions in the city. The diurnal statistical patterns suggested that reduced
 579 traffic emissions were most likely an important factor in causing the observed changes. It is expected
 580 that traffic intensity changed in a modest manner in the city centre during the time interval of interest,
 581 so our results indicate that the reductions is most likely related to lower emission factors. This appears
 582 to follow some changes of sulfur content in fuels and control measures on emissions for on-road heavy-
 583 duty diesel vehicles. Introduction of better particle filters in diesel cars, cleaner fuel and more
 584 sophisticated diesel engines could also contribute. Modernised technologies in residential and household
 585 heating could also contribute. The magnitude of the traffic emission reduction cannot be completely
 586 conclusive in all aspects for the moment and further investigations are planned on the basis of the present
 587 results. The changes appear to have responded to both the policy on urban air quality and the influence
 588 of economic circumstances of inhabitants. Excitingly, the mean ages of passenger cars and busses in
 589 Hungary increased during the years under investigation. The exact explanation and confirmation of the
 590 decrease require continuation of the related measurements with independent experimental systems and
 591 further dedicated studies. The present results can be also used for evaluating the effectiveness of present
 592 and prospective mitigation policies.

593 The diurnal statistical patterns can be also utilized in interpreting some properties of NPF events in urban
594 environments, and in explaining time evolution of particle number concentration. As a result of GLMM,
595 we could, for instance, give a parametrization for predicting particle concentrations in different size
596 fractions. Models similar to those developed in the present study could be used for other particle sizes or
597 locations as well. The same parameterization could be used at least in areas with similar concentration
598 levels of particles and pollutants, while the extrapolation of the results to cleaner or more polluted
599 environments needs to be confirmed before the use. Conjugate or linked parameterizations to be
600 developed for varying environments can be implemented as a part of atmospheric models to predict the
601 concentrations of climatically active particles in order to reduce their extensive computational times. In
602 addition, this could also contribute to solving some current uncertain issues in the theoretical description
603 of NPF and growth process, particularly when predicting cloud condensation nuclei concentrations.

604 **Data availability.** The observational data used in this paper are available on request from the corresponding author
605 Imre Salma.

606 **Author contributions.** IS and SM formulated the original concept; ZN, VV, TW and IS collected and processed
607 the experimental data; SM, VL and TY were responsible for the statistical data analyses and their physical basis;
608 SM and IS interpreted the results; IS and SM wrote the manuscript with contributions from all co-authors.

609 **Competing interest.** The authors declare that they have no conflict of interest.

610 **Financial support.** The research was supported by the National Research, Development and Innovation Office,
611 Hungary (contracts K116788, PD124283 and K132254), by the János Bolyai Research Scholarship of the
612 Hungarian Academy of Sciences (ZN) and by the European Regional Development Fund and the Hungarian
613 Government (GINOP-2.3.2-15-2016-00028), The Nessling Foundation, The Academy of Finland Centre of
614 Excellence (grant no. 307331) and The Academy of Finland Competitive funding to strengthen university research
615 profiles (PROFI) for the University of Eastern Finland (grant no. 325022) and Academy of Finland project (grant
616 no. 299544)

617 **References**

- 618 Aalto, P., Hämeri, K., Becker, E., Weber, R., Salm, J., Mäkelä, J., Hoell, C., O'Dowd, C., Karlsson, H., Väkevä,
619 M., Koponen, I. K., Buzorius, G., and Kulmala, M.: Physical characterization of aerosol particles during
620 nucleation events, *Tellus*, 53B, 344–358, 2001.
- 621 Aalto, P., Hämeri, K., Paatero, P., Kulmala, M., Bellander, T., Berglind, N., Bouso, L., Castaño-Vinyals, G.,
622 Sunyer, J., Cattani, G., Marconi, A., Cyrus, J., von Klot, S., Peters, A., Zetzsche, K., Lanki, T., Pekkanen, J.,
623 Nyberg, F., Sjövall, B., and Forastiere, F.: Aerosol particle number concentration measurements in five
624 European cities using TSI-3022 condensation particle counter over a three-year period during health effects of
625 air pollution on susceptible subpopulations, *J. Air Waste Manage. Assoc.*, 55, 1064–1076, 2005.
- 626 Asmi, A., Collaud Coen, M., Ogren, J. A., Andrews, E., Sheridan, P., Jefferson, A., Weingartner, E., Baltensperger,
627 U., Bukowiecki, N., Lihavainen, H., Kivekas, N., Asmi, E., Aalto, P. P., Kulmala, M., Wiedensohler, A.,
628 Birmili, W., Hamed, A., O'Dowd, C., Jennings, S. G., Weller, R., Flentje, H., Fjaeraa, A. M., Fiebig, M., Myhre,
629 C. L., Hallar, A. G., Swietlicki, E., Kristensson, A., and Laj, P.: Aerosol decadal trends - Part 2: In-situ aerosol
630 particle number concentrations at GAW and ACTRIS stations, *Atmos. Chem. Phys.*, 13, 895–916, 2013.

631 Avino, P., Casciardi, S., Fanizza, C., and Manigrasso, M.: Deep investigation of ultrafine particles in urban air,
632 *Aerosol Air Qual. Res.*, 11, 654–663, 2011.

633 Birmili, W., Wiedensohler, A., Heintzenberg, J., and Lehmann, K.: Atmospheric particle number size distribution
634 in central Europe: Statistical relations to air masses and meteorology, *J. Geophys. Res., Atmospheres*,
635 106(D23), 32005-18, 2001.

636 Braakhuis, H. M., Park, M. V., Gosens, I., De Jong, W. H., and Cassee, F. R.: Physicochemical characteristics of
637 nanomaterials that affect pulmonary inflammation, *Part. Fibre Toxicol.*, 11:18, doi: 10.1186/1743-8977-11-18,
638 2014.

639 Brines, M., Dall'Osto, M., Beddows, D. C. S., Harrison, R. M., Gómez-Moreno, F., Núñez, L., Artñano, B.,
640 Costabile, F., Gobbi, G. P., Salimi, F., Morawska, L., Sioutas, C., and Querol, X.: Traffic and nucleation events
641 as main sources of ultrafine particles in high-insolation developed world cities, *Atmos. Chem. Phys.* 15, 5929–
642 5945, 2015.

643 Cassee, F. R., Héroux, M.-E., Gerlofs-Nijland, M. E., and Kelly, F. J.: Particulate matter beyond mass: recent
644 health evidence on the role of fractions, chemical constituents and sources of emission, *Inhal. Toxicol.* 25,
645 802–812, 2013.

646 Carslaw, K. S., Lee, L. A., Reddington, C. L., Pringle, K. J., Rap, A., Forster, P. M., Mann, G. W., Spracklen, D.
647 V., Woodhouse, M. T., Regayre, L. A., and Pierce, J. R.: Large contribution of natural aerosols to uncertainty
648 in indirect forcing, *Nature*, 503, 67–71, 2013.

649 Dada, L., Ylivinkka, I., Baalbaki, R., Li, Ch., Guo, Y., Yan, Ch., Yao, L., Sarnela, N., Jokinen, T., Daellenbach,
650 K. D., Yin, R., Deng, Ch., Chu, B., Nieminen, T., Kontkanen, J., Stolzenburg, D., Sipilä, M., Hussein, T.,
651 Paasonen, P., Bianchi, F., Salma, I., Weidinger, T., Pikridas, M., Sciare, J., Jiang, J., Liu, Y., Petäjä, T.,
652 Kerminen, V.-M., and Kulmala, M.: Sources and sinks driving sulphuric acid concentrations in contrasting
653 environments: implications on proxy calculations, *Atmos. Chem. Phys. Discuss.*, under evaluation, 2020.

654 Dal Maso, M., Kulmala, M., Lehtinen, K. E. J., Mäkelä, J. M., Aalto, P. P., and O'Dowd, C.: Condensation and
655 coagulation sinks and formation of nucleation mode particles in coastal and boreal forest boundary layers, *J.*
656 *Geophys. Res.*, 107(19D), 8097, 10.1029/2001jd001053, 2002.

657 Dal Maso, M., Kulmala, M., Riipinen, I., Wagner, R., Hussein, T., Aalto, P. P., and Lehtinen, K. E. J.: Formation
658 and growth of fresh atmospheric aerosols: eight years of aerosol size distribution data from SMEAR II,
659 Hyytiälä, Finland, *Boreal Environ. Res.*, 10, 323–336, 2005.

660 Dall'Osto, M., Querol, X., Alastuey, A., O'Dowd, C., Harrison, R. M., Wenger, J., and Gómez-Moreno, F. J.: On
661 the spatial distribution and evolution of ultrafine particles in Barcelona, *Atmos. Chem. Phys.*, 13, 741–759,
662 2013.

663 Directive 2009/30/EC, Official Journal of the European Union, L 140, EN, 88–113, 5. 6. 2009.

664 Dunne, E. M., Gordon, H., Kürten, A., Almeida, J., Duplissy, J., Williamson, C., Ortega, I. K., Pringle, K. J.,
665 Adamov, A., Baltensperger, U., Barmet, P., Benduhn, F., Bianchi, F., Breitenlechner, M., Clarke, A., Curtius,
666 J., Dommen, J., Donahue, N. M., Ehrhart, S., Flagan, R. C., Franchin, A., Guida, R., Hakala, J., Hansel, A.,
667 Heinritzi, M., Jokinen, T., Kangasluoma, J., Kirkby, J., Kulmala, M., Kupc, A., Lawler, M. J., Lehtipalo, K.,
668 Makhmutov, V., Mann, G., Mathot, S., Merikanto, J., Miettinen, P., Nenes, A., Onnela, A., Rap, A.,
669 Reddington, C. L. S., Riccobono, F., Richards, N. A. D., Rissanen, M. P., Rondo, L., Sarnela, N.,
670 Schobesberger, S., Sengupta, K., Simon, M., Sipilä, M., Smith, J. N., Stozkhov, Y., Tomé, A., Tröstl, J.,
671 Wagner, P. E., Wimmer, D., Winkler, P. M., Worsnop, D. R., and Carslaw, K. S.: Global atmospheric particle
672 formation from CERN CLOUD measurements, *Science* 354, 1119–1124, 2016.

673 Durbin, J. and Koopman, S. J.: Time series analysis by state space methods, Oxford University Press, Oxford,
674 2012.

675 Giechaskiel, B., Lahde, T., Suarez-Bertoa, R., Clairotte, M., Grigoratos, T., Zardini, A., Perujo, A., and Martini,
676 G.: Particle number measurements in the European legislation and future JRC activities, *Combustion Engines*,
677 174, 3–16, 2018.

678 Gordon, H., Sengupta, K., Rap, A., Duplissy, J., Frege, C., Williamson, C., Heinritzi, M., Simon, M., Yan, C.,
679 Almeida, J., Tröstl, J., Nieminen, T., Ortega, I. K., Wagner, R., Dunne, E. M., Adamov, A., Amorim, A.,
680 Bernhammer, A. K., Bianchi, F., Breitenlechner, M., Brilke, S., Chen, X., Craven, J. S., Dias, A., Ehrhart, S.,
681 Fischer, L., Flagan, R. C., Franchin, A., Fuchs, C., Guida, R., Hakala, J., Hoyle, C. R., Jokinen, T., Junninen,
682 H., Kangasluoma, J., Kim, J., Kirkby, J., Krapf, M., Kürten, A., Laaksonen, A., Lehtipalo, K., Makhmutov, V.,
683 Mathot, S., Molteni, U., Monks, S. A., Onnela, A., Peräkylä, O., Piel, F., Petäjä, T., Praplan, A. P., Pringle, K.

684 J., Richards, N. A. D., Rissanen, M. P., Rondo, L., Sarnela, N., Schobesberger, S., Scott, C. E., Seinfeld, J. H.,
685 Sharma, S., Sipilä, M., Steiner, G., Stozhkov, Y., Stratmann, F., Tomé, A., Virtanen, A., Vogel, A. L., Wagner,
686 A. C., Wagner, P. E., Weingartner, E., Wimmer, D., Winkler, P. M., Ye, P., Zhang, X., Hansel, A., Dommen,
687 J., Donahue, N. M., Worsnop, D. R., Baltensperger, U., Kulmala, M., Curtius, J., and Carslaw, K. S.: Reduced
688 anthropogenic aerosol radiative forcing caused by biogenic new particle formation, *Proc. Natl. Acad. Sci.*
689 *U.S.A.*, 113, 12053–12058, 2016.

690 Guo, H., Wang, D. W., Cheung, K., Ling, Z. H., Chan, C. K., and Yao, X. H.: Observation of aerosol size
691 distribution and new particle formation at a mountain site in subtropical Hong Kong, *Atmos. Chem. Phys.*, 12,
692 9923–9939, <https://doi.org/10.5194/acp-12-9923-2012>, 2012.

693 Hamed, A., H. Korhonen, S.-L. Sihto, J. Joutsensaari, H. Järvinen, T. Petäjä, F. Arnold, T. Nieminen, M. Kulmala,
694 J. N. Smith, K. E. J. Lehtinen, A. Laaksonen: The role of relative humidity in continental new particle
695 formation, *J. Geophys. Res.*, 116, D03202, doi:10.1029/2010JD014186, 2011.

696 Hussein, T., Puustinen, A., Aalto, P. P., Mäkelä, J. M., Hämeri, K., and Kulmala, M.: Urban aerosol number size
697 distributions, *Atmos. Chem. Phys.*, 4, 391–411, 2004.

698 Hyvönen, S., Junninen, H., Laakso, L., Dal Maso, M., Grönholm, T., Bonn, B., Keronen, P., Aalto, P., Hiltunen,
699 V., Pohja, T., Launiainen, S., Hari, P., Mannila, H., and Kulmala, M.: A look at aerosol formation using data
700 mining techniques, *Atmos. Chem. Phys.*, 5, 3345–3356, 2005.

701 Károssy, Cs.: A Kárpát-medence Péczely-féle makroszinoptikus időjárási helyzeteinek katalógusa 1881–2015
702 (Catalogue of the Péczely macrosynoptic weather types for the Carpathian Basin 1881–2015, in Hungarian),
703 OSKAR Kiadó, Budapest, 2016.

704 Kerminen, V.-M., Paramonov, M., Anttila, T., Riipinen, I., Fountoukis, C., Korhonen, H., Asmi, E., Laakso, L.,
705 Lihavainen, H., Swietlicki, E., Svenningsson, B., Asmi, A., Pandis, S. N., Kulmala, M., and Petäjä, T.: Cloud
706 condensation nuclei production associated with atmospheric nucleation: a synthesis based on existing literature
707 and new results, *Atmos. Chem. Phys.*, 12, 12037–12059, 2012.

708 Kerminen, V.-M., Chen, X., Vakkari, V., Petäjä, T., Kulmala, M., and Bianchi, F.: Atmospheric new particle
709 formation and growth: review of field observations, *Environ. Res. Lett.*, 13 (2018) 103003, 2018.

710 KSH, National register of road vehicles (in Hungarian), Hungarian Central Statistical Office, Budapest, 2019.

711 Kulmala, M., Dal Maso, M., Mäkelä, J. M., Pirjola, L., Väkevä, M., Aalto, P., Miikkulainen, P., Hämeri, K., and
712 O'Dowd, C. D.: On the formation, growth and composition of nucleation mode particles, *Tellus B*53, 479–490,
713 2001.

714 Kulmala, M., Petäjä, T., Nieminen, T., Sipilä, M., Manninen, H. E., Lehtipalo, K., Dal Maso, M., Aalto, P. P.,
715 Junninen, H., Paasonen, P., Riipinen, I., Lehtinen, K. E. J., Laaksonen, A., and Kerminen, V.-M.: Measurement
716 of the nucleation of atmospheric aerosol particles, *Nat. Protoc.*, 7, 1651–1667, doi:10.1038/nprot.2012.091,
717 2012.

718 Kulmala, M., Kontkanen, J., Junninen, H., Lehtipalo, K., Manninen, H. E., Nieminen, T., Petäjä, T., Sipilä, M.,
719 Schobesberger, S., Rantala, P., Franchin, A., Jokinen, T., Järvinen, E., Äijälä, M., Kangasluoma, J., Hakala, J.,
720 Aalto, P. P., Paasonen, P., Mikkilä, J., Vanhanen, J., Aalto, J., Hakola, H., Makkonen, U., Ruuskanen, T.,
721 Mauldin, R. L. III, Duplissy, J., Vehkamäki, H., Bäck, J., Kortelainen, A., Riipinen, I., Kurtén, T., Johnston,
722 M. V., Smith, J. N., Ehn, M., Mentel, T. F., Lehtinen, K. E. J., Laaksonen, A., Kerminen, V.-M., and Worsnop,
723 D. R.: Direct observations of atmospheric aerosol nucleation, *Science*, 339, 943–946, 2013.

724 Kulmala, M., Petäjä, T., Ehn, M., Thornton, J., Sipilä, M., Worsnop, D. R., and Kerminen, V.-M.: Chemistry of
725 atmospheric nucleation: On the recent advances on precursor characterization and atmospheric cluster
726 composition in connection with atmospheric new particle formation, *Annu. Rev. Phys. Chem.*, 65, 21–37,
727 2014.

728 Kulmala, M., Kerminen, V. M., Petäjä, T., Ding, A. J., and Wang, L.: Atmospheric gas-to-particle conversion:
729 why NPF events are observed in megacities, *Faraday Discuss.*, doi:10.1039/C6FD00257A, 2017.

730 Laine, M.: Introduction to Dynamic Linear Models for Time Series Analysis. In: Montillet, J. P., Bos, M. (eds),
731 *Geodetic Time Series Analysis in Earth Sciences*, Springer, pp. 139–156, 2020.

732 Maheras, P., Tolika, K., Tegoulías, I., Anagnostopoulou, Ch., Szpirosz, K. Károssy, Cs., and Makra, L.:
733 Comparison of an automated classification system with an empirical classification of circulation patterns over
734 the Pannonian basin, Central Europe, *Meteorol. Atmos. Phys.*, <https://doi.org/10.1007/s00703-018-0601-x>,
735 2018.

736 Makkonen, R., Asmi, A., Korhonen, H., Kokkola, H., Järvenoja, S., Räisänen, P., Lehtinen, K. E. J., Laaksonen,
737 A., Kerminen, V.-M., Järvinen, H., Lohmann, U., Bennartz, R., Feichter, J., and Kulmala, M.: Sensitivity of
738 aerosol concentrations and cloud properties to nucleation and secondary organic distribution in ECHAM5-
739 HAM global circulation model, *Atmos. Chem. Phys.*, 9, 1747–1766, 2009.

740 Masiol, M., Squizzato, S., Chalupa, D., Utell, M. J., Rich, D. Q., and Hopke, P. K.: Long-term trends in submicron
741 particle concentrations in a metropolitan area of the northeastern United States, *Sci. Total Environ.*, 633, 59–
742 70, 2018.

743 McCulloch, C. E., Searle, S. R., and Neuhaus, J. M.: *Generalized, linear, and mixed models*, 2nd ed., Wiley, New
744 York, 2008.

745 McFiggans, G., Mentel, T. F., Wildt, J., Pullinen, I., Kang, S., Kleist, E., Schmitt, S., Springer, M., Tillmann, R.,
746 Wu, C., Zhao, D., Hallquist, M., Faxon, C., Le Breton, M., Hallquist, A. M., Simpson, D., Bergstroem, R.,
747 Jenkin, M. E., Ehn, M., Thornton, J. A., Alfarra, M. R., Bannan, T. J., Percival, C. J., Priestley, M., Topping,
748 D., and Kiendler-Scharr, A.: Secondary organic aerosol reduced by mixture of atmospheric vapours, *Nature*,
749 565, 587–593, 2019.

750 Merikanto, J., Spracklen, D. V., Mann, G. W., Pickering, S. J., and Carslaw, K. S.: Impact of nucleation on global
751 CCN, *Atmos. Chem. Phys.*, 9, 8601–8616, 2009.

752 Mikkonen, S., Lehtinen, K. E. J., Hamed, A., Joutsensaari, J., Facchini, M. C., and Laaksonen, A.: Using
753 discriminant analysis as a nucleation event classification method, *Atmos. Chem. Phys.*, 6, 5549–5557,
754 <https://doi.org/10.5194/acp-6-5549-2006>, 2006.

755 Mikkonen, S., Korhonen, H., Romakkaniemi, S., Smith, J. N., Joutsensaari, J., Lehtinen, K. E. J., Hamed, A.,
756 Breider, T. J., Birmili, W., Spindler, G., Plass-Duelmer, C., Facchini, M. C., and Laaksonen, A.:
757 Meteorological and trace gas factors affecting the number concentration of atmospheric Aitken ($D_p=50$ nm)
758 particles in the continental boundary layer: parameterization using a multivariate mixed effects model, *Geosci.*
759 *Model Dev.*, 4, 1–13, <https://doi.org/10.5194/gmd-4-1-2011>, 2011a.

760 Mikkonen, S., Romakkaniemi, S., Smith, J. N., Korhonen, H., Petäjä, T., Plass-Duelmer, C., Boy, M., McMurry,
761 P. H., Lehtinen, K. E. J., Joutsensaari, J., Hamed, A., Mauldin III, R. L., Birmili, W., Spindler, G., Arnold, F.,
762 Kulmala, M., and Laaksonen, A.: A statistical proxy for sulphuric acid concentration, *Atmos. Chem. Phys.*, 11
763 11319–11334, <https://doi.org/10.5194/acp-11-11319-2011>, 2011b.

764 Mikkonen, S., Laine, M., Mäkelä, H. M., Gregow, H., Tuomenvirta, H., Lahtinen, M., Laaksonen, A.: Trends in
765 the average temperature in Finland, 1847–2013, *Stoch. Environ. Res. Risk Ass.*, 29, 1521–1529, 2015.

766 Moore, K. F., Ning, Z., Ntziachristos, L., Schauer, J. J., and Sioutas, C.: Daily variation in the properties of urban
767 ultrafine aerosol - Part I: Physical characterization and volatility, *Atmos. Environ.*, 41, 8633–8646, 2007.

768 Moosmuller, H., Chakrabarty, R. K. and Arnott, W.: Aerosol light absorption and its measurement: A review, *J.*
769 *Quant. Spectrosc. Radiat. Transf.*, 110, 844–878, 2009.

770 Németh, Z. and Salma, I.: Spatial extension of nucleating air masses in the Carpathian Basin, *Atmos. Chem. Phys.*,
771 14, 8841–8848, 2014.

772 Németh, Z., Rosati, B., Žíková, N., Salma, I., Bozó, L., Dameto de España, C., Schwarz, J., Ždímal, V., and
773 Wonaschütz, A.: Comparison of atmospheric new particle formation and growth events in three Central
774 European cities, *Atmos. Environ.*, 178, 191–197, 2018.

775 Nieminen, T., Asmi, A., Dal Maso, M., P. Aalto, P., Keronen, P., Petäjä, T., Kulmala, M. & Kerminen, V.-M.:
776 Trends in atmospheric new-particle formation: 16 years of observations in a boreal-forest environment. *Boreal*
777 *Env. Res.* 19 (suppl. B): 191–214, 2014.

778 Nieminen, T., Kerminen, V.-M., Petäjä, T., Aalto, P. P., Arshinov, M., Asmi, E., Baltensperger, U., Beddows, D.
779 C. S., Beukes, J. P., Collins, D., Ding, A., Harrison, R. M., Henzing, B., Hooda, R., Hu, M., Hörrak, U.,
780 Kivekäs, N., Komsaare, K., Krejci, R., Kristensson, A., Laakso, L., Laaksonen, A., Leaitch, W. R., Lihavainen,
781 H., Mihalopoulos, N., Németh, Z., Nie, W., O'Dowd, C., Salma, I., Sellegri, K., Svenningsson, B., Swietlicki,
782 E., Tunved, P., Ulevicius, V., Vakkari, V., Vana, M., Wiedensohler, A., Wu, Z., Virtanen, A., and Kulmala,
783 M.: Global analysis of continental boundary layer new particle formation based on long-term measurements,
784 *Atmos. Chem. Phys.*, 18, 14737–14756, 2018.

785 Oberdörster, G., Oberdörster, E., and Oberdörster, J.: Nanotoxicology: an emerging discipline evolving from
786 studies of ultrafine particles, *Environ. Health Perspect.*, 113, 823–839, 2005.

787 Ohlwein, S., Kappeler, R., Joss, M. K., Künzli, N., and Hoffmann, B.: Health effects of ultrafine particles: a
788 systematic literature review update of epidemiological evidence, *Int. J. Public Health*, 685, 547–559, 2019.

789 Ostro, B., Hu, J., Goldberg, D., Reynolds, P., Hertz, A., Bernstein, L., and Kleeman, M. J.: Associations of
790 mortality with long-term exposures to fine and ultrafine particles, species and sources: results from the
791 California teachers study cohort, *Environ. Health Perspect.*, 123, 549–556, 2015.

792 Paasonen, P., Kupiainen, K., Klimont, Z., Visschedijk, A., Denier van der Gon, H. A. C., and Amann, M.:
793 Continental anthropogenic primary particle number emissions, *Atmos. Chem. Phys.*, 16, 6823–6840, 2016.

794 Péczely, Gy.: Grosswetterlagen in Ungarn (Large-scale weather situations in Hungary, in German), Publication of
795 the Hungarian Meteorological Institute, 30, pp. 86, Budapest, 1957.

796 Petäjä, T., Mauldin, III, R. L., Kosciuch, E., McGrath, J., Nieminen, T., Paasonen, P., Boy, M., Adamov, A.,
797 Kotiaho, T., and Kulmala, M.: Sulfuric acid and OH concentrations in a boreal forest site, *Atmos. Chem. Phys.*,
798 9, 7435–7448, 2009.

799 Petris, G., Petrone, S., and Campagnoli, P.: *Dynamic linear models*, Springer, New York, 2009.

800 Pinheiro, J.C., and Bates, D.M.: *Mixed-Effects Models in S and S-PLUS*, Springer, 2000.

801 Platt, S. M., El Haddad, I., Pieber, S. M., Zardini, A. A., Suarez-Bertoa, R., Clairotte, M., Daellenbach, K. R.,
802 Huang, R.-J., Slowik, J. G., Hellebust, S., Temime-Roussel, B., Marchand, N., de Gouw, J., Jimenez, J. L.,
803 Hayes, P. L., Robinson, A. L., Baltensperger, U., Astorga, C., and Prévôt, A. S. H.: Gasoline cars produce
804 more carbonaceous particulate matter than modern filter-equipped diesel cars, *Sci. Rep.*, 7, 4926, 2017,
805 <https://doi.org/10.1038/s41598-017-03714-9>.

806 Pöschl, U., Rudich, Y., and Ammann, M.: Kinetic model framework for aerosol and cloud surface chemistry and
807 gas-particle interactions – Part 1: General equations, parameters, and terminology, *Atmos. Chem. Phys.*, 7,
808 5989–6023, 2007.

809 Raes, F., Van Dingenen, R., Vignati, E., Wilson, J., Putaud, J. P., Seinfeld, J. H., and Adams, P.: Formation and
810 cycling of aerosol in the global troposphere, *Atmos. Environ.*, 34, 4215–4240, 2000.

811 Rich, D. Q., Zareba, W., Beckett, W., Hopke, P. K., Oakes, D., Frampton, M. W., Bisognano, J., Chalupa, D.,
812 Bausch, J., O'Shea, K., Wang, Y., and Utell, M. J.: Are ambient ultrafine, accumulation mode, and fine particles
813 associated with adverse cardiac responses in patients undergoing cardiac rehabilitation?, *Environ. Health
814 Perspect.*, 120, 1162–1169, 2012.

815 Saha, P. K., Robinson, E. S., Shah, R. U., Zimmerman, N., Apte, J. S., Robinson, A. L., and Presto, A. A.: Reduced
816 ultrafine particle concentration in urban air: changes in nucleation and anthropogenic emissions, *Environ. Sci.
817 Technol.*, 52, 6798–6806, 2018.

818 Salma, I., Borsós, T., Weidinger, T., Aalto, P., Hussein, T., Dal Maso, M., and Kulmala, M.: Production, growth
819 and properties of ultrafine atmospheric aerosol particles in an urban environment, *Atmos. Chem. Phys.*, 11,
820 1339–1353, 2011.

821 Salma, I., Borsós, T., Németh, Z., Weidinger, T., Aalto, T., and Kulmala, M.: Comparative study of ultrafine
822 atmospheric aerosol within a city, *Atmos. Environ.*, 92, 154–161, 2014.

823 Salma, I., Németh, Z., Weidinger, T., Kovács, B., and Kristóf, G.: Measurement, growth types and shrinkage of
824 newly formed aerosol particles at an urban research platform, *Atmos. Chem. Phys.*, 16, 7837–7851, 2016a.

825 Salma, I., Németh, Z., Kerminen, V. M., Aalto, P., Nieminen, T., Weidinger, T., Molnár, Á., Imre, K., and
826 Kulmala, M.: Regional effect on urban atmospheric nucleation, *Atmos. Chem. Phys.*, 16, 8715–8728, 2016b.

827 Salma, I., Varga, V., and Németh, Z.: Quantification of an atmospheric nucleation and growth process as a single
828 source of aerosol particles in a city, *Atmos. Chem. Phys.*, 17, 15007–15017, 2017.

829 Salma, I. and Németh, Z.: Dynamic and timing properties of new aerosol particle formation and consecutive
830 growth events, *Atmos. Chem. Phys.*, 19, 5835–5852, 2019.

831 Salvo, A., Brito, J., Artaxo, P., and Geiger, F. M.: Reduced ultrafine particle levels in São Paulo's atmosphere
832 during shifts from gasoline to ethanol use, *Nat. Commun.*, 8, 77, DOI: 10.1038/s41467-017-00041-5, 2017.

833 Schmid, O. and Stoeger, T.: Surface area is the biologically most effective dose metric for acute nanoparticle
834 toxicity in the lung, *J. Aerosol Sci.*, 99, 133–143, 2016.

835 Sihto, S.-L., Mikkilä, J., Vanhanen, J., Ehn, M., Liao, L., Lehtipalo, K., Aalto, P. P., Duplissy, J., Petäjä, T.,
836 Kerminen, V.-M., Boy, M., and Kulmala, M.: Seasonal variation of CCN concentrations and aerosol activation
837 properties in boreal forest, *Atmos. Chem. Phys.*, 11, 13269–13285, 2011.

838 Sipilä, M., Berndt, T., Petäjä, T., Brus, D., Vanhanen, J., Stratmann, F., Patokoski, J., Mauldin, R. L. 3rd,
839 Hyvärinen, A. P., Lihavainen, H., and Kulmala, M.: The role of sulfuric acid in atmospheric nucleation,
840 *Science*, 327(5970), 1243–6. doi: 10.1126/science.1180315, 2010.

841 Spracklen, D. V., Carslaw, K. S., Merikanto, J., Mann, G. W., Reddington, C. L., Pickering, S., Ogren, J. A.,
842 Andrews, E., Baltensperger, U., Weingartner, E., Boy, M., Kulmala, M., Laakso, L., Lihavainen, H., Kivekäs,
843 N., Komppula, M., Mihalopoulos, N., Kouvarakis, G., Jennings, S. G., O'Dowd, C., Birmili, W., Wiedensohler,

844 A., Weller, R., Gras, J., Laj, P., Sellegri, K., Bonn, B., Krejčí, R., Laaksonen, A., Hamed, A., Minikin, A.,
845 Harrison, R. M., Talbot, R., and Sun, J.: The contribution of boundary layer nucleation events to total particle
846 concentrations on regional and global scales, *Atmos. Chem. Phys.*, 6, 5631–5648, 2006.

847 Sun, J., Birmili, W., Hermann, M., Tuch, T., Weinhold, K., Merkel, M., Rasch, F., Müller, T., Schladitz, A.,
848 Bastian, S., Löschau, G., Cyrus, J., Gu, J., Flentje, H., Briel, B., Asbach, C., Kaminski, H., Ries, L., Sohmer,
849 R., Gerwig, H., Wirtz, K., Meinhardt, F., Schwerin, A., Bath, O., Ma, N., and Wiedensohler, A.: Decreasing
850 trends of particle number and black carbon mass concentrations at 16 observational sites in Germany from
851 2009 to 2018, *Atmos. Chem. Phys.*, 20, 7049–7068, doi:10.5194/acp-20-7049-2020, 2020.

852 Wehner, B. and Wiedensohler, A.: Long term measurements of submicrometer urban aerosols: statistical analysis
853 for correlations with meteorological conditions and trace gases, *Atmos. Chem. Phys.*, 3, 867–879, 2003

854 Wihersaari, H., Pirjola, L., Karjalainen, P., Saukko, E., Kuuluvainen, H., Kulmala, K., Keskinen, J. and Rönkkö,
855 T.: Particulate emissions of a modern diesel passenger car under laboratory and real-world transient driving
856 conditions, *Environ. Pollut.*, 265, 114948, doi:10.1016/j.envpol.2020.114948, 2020.

857 Wiedensohler, A., Cheng, Y. F., Nowak, A., Wehner, B., Achtert, P., Berghof, M., Birmili, W., Wu, Z. J., Hu, M.,
858 Zhu, T., Takegawa, N., Kita, K., Kondo, Y., Lou, S. R., Hofzumahaus, A., Holland, F., Wahner, A., Gunthe,
859 S. S., Rose, D., Su, H., and Pöschl, U.: Mobility particle size spectrometers: harmonization of technical
860 standards and data structure to facilitate high quality long-term observations of atmospheric particle number
861 size distributions, *Atmos. Meas. Tech.*, 5, 657–685, 2012.

862 Willmott, C. J., Matsuura, K., and Robeson, S. M.: Ambiguities inherent in sums-of-squares-based error statistics,
863 *Atmos. Environ.*, 43, 749–752, doi:10.1016/j.atmosenv.2008.10.005, 2009.

864 Yu, F., Luo, G., Bates, T. S., Anderson, B., Clarke, A., Kapustin, V., Yantosca, R. M., Wang, Y., and Wu, S.:
865 Spatial distributions of particle number concentrations in the global troposphere: simulations, observations,
866 and implications for nucleation mechanisms, *J. Geophys. Res.*, 115, D17205, doi:10.1029/2009JD013473,
867 2010.

868 Zaidan, M. A., Haapasilta, V., Relan, R., Paasonen, P., Kerminen, V.-M., Junninen, H., Kulmala, M., and Foster,
869 A. S.: Exploring non-linear associations between atmospheric new-particle formation and ambient variables: a
870 mutual information approach, *Atmos. Chem. Phys.*, 18, 12699–12714, 2018.

871 Zhang, R., Wang, G., Guo, S., Zamora, M. L., Ying, Q., Lin, Y., Wang, W., Hu, M., and Wang, Y.: Formation of
872 urban fine particulate matter, *Chem. Rev.*, 115, 3803–3855, 2015.